Paper No. 02-2701

Pile Monitoring with Fiber Optic Sensors During Axial Compression, Pullout, and Flexure Tests

Branko Glisic, Daniele Inaudi, and Claire Nan

A full-scale on-site test represents an ideal way to check a hypothesis and to determine the real behavior of structures, especially in cases in which some uncertainties cannot be reduced otherwise. To perform the test successfully it is necessary to monitor the parameters that representatively describe the structural behavior. In the case of piles, axial compression, pullout, and flexure tests cover all load combinations that may appear in service. To assess the foundation performance at a semiconductor production facility, two sets of piles with three piles in each set were tested. The monitored parameters were average strains, registered in several segments over the whole length of each pile using long-gauge fiber optic sensors. This type of sensor, combined in appropriate topologies, gives rich information concerning the piles' behavior and soil properties. The monitoring method is presented and its performances through the results of the tests are discussed. This method allowed the determination of the Young modulus of the piles, the occurrence of cracks, the normal force distribution, and the ultimate load capacity in the case of axial compression and pullout tests, as well as the curvature distribution, horizontal displacement, deformed shape, and damage localization in the case of the flexure tests. Moreover, the pile–soil friction distributions, the quality of soil, and the pile tip force were estimated. The advantage of the presented method resides in the use of long-gauge sensors, which are insensitive to local structural defects like crack openings or air pockets and allow the collection of data on a global structural level and not on a local material level.

A new semiconductor production facility in the Tainan Scientific Park, Taiwan, is to be founded on a soil consisting mainly of clay and sand with poor mechanical properties (see Figure 1). Natural water content is approximately 20% to 25%. Adequate functioning of such a facility is possible only if a high stability of its foundation is guaranteed. It was estimated that approximately 3,000 piles would be necessary at that site. To assess the foundation performance, full-scale on-site axial compression, pullout, and flexure tests were performed. Fiber optic long-gauge sensors were used to monitor the behavior of the six piles being tested.

Long-gauge fiber optic sensors have opened new possibilities for structural monitoring (*1*). Being long-gauge, the sensors are insensitive to the local defects of materials, and therefore allow monitoring at a global, structural level. Being fiber optic based, they offer high resolution and accuracy as well as excellent long-term stability. When combined in appropriate topologies, they not only offer pure deformation (average strain) measurements, but also make it possible to determine other important parameters such as curvature, deformed shape, crack detection and localization, ultimate load capacity, Young modulus, and soil properties. More than 70 sensors of this type were used for the tests.

The aim of this article is to present the monitoring method and the results of the tests. Because of length limitations, only the most important results are presented.

B. Glisic and D. Inaudi, SMARTEC SA, Via Pobbiette 11, 6928 Manno, Switzerland. C. Nan, RouteAero Technology and Engineering, 12F-1, 56 Nanking E. Road, Sec. 5, Taipei 105, Taiwan, R.O.C.

DESCRIPTION OF TESTS

Two sets of reverse, cast-in-place piles, respectively located on the east side and west side of the future facility, were tested. Each set consisted of three piles, and each pile in a set was tested to a single load case [i.e., compression (according to ASTM D1143-B1), uplift (according to ASTM D3689-B3), or horizontal force (according to ASTM D3966-90)]. All piles had the same dimensions (a diameter of 1.20 m and length of 35 m) and were designed and constructed to have the same mechanical properties. The compressive strength of 3-week-old concrete samples was 24.5 MPa and the calculated compression and uplift capacity were 365 tons and 220 tons, respectively. The dimensions of piles, rebar layout, and simplified soil mechanical properties are presented in Figure 1.

The load was applied stepwise using hydraulic jacks and according to a predetermined program. The magnitude of the applied load was monitored on the hydraulic scale of the loading setup. Each level of load was maintained during a period whose length was determined depending on the load level. After the maximum load was reached, the piles were unloaded, again stepwise, according to the program.

In order to monitor the behavior of the piles during testing, each pile was instrumented with long-gauge fiber optic sensors combined in appropriate topologies. In addition, the displacement of the head of the pile was recorded using linear variable differential transformers (LVDTs). The measurement readings were performed immediately after each step of load and several times afterwards, while the load level was maintained. The schedules for loading and measurements are presented in Table 1. The numbers in the columns labeled "measurements" indicate the elapsed time in minutes after reaching the target load.

DESCRIPTION OF MONITORING SYSTEM

The monitoring system used in the presented tests is called SOFO (French acronym for surveillance d'ouvrages par fibres optiques—structural monitoring using optical fibers) and is based on low-coherence interferometry in optical fiber sensors (*2*). The functioning

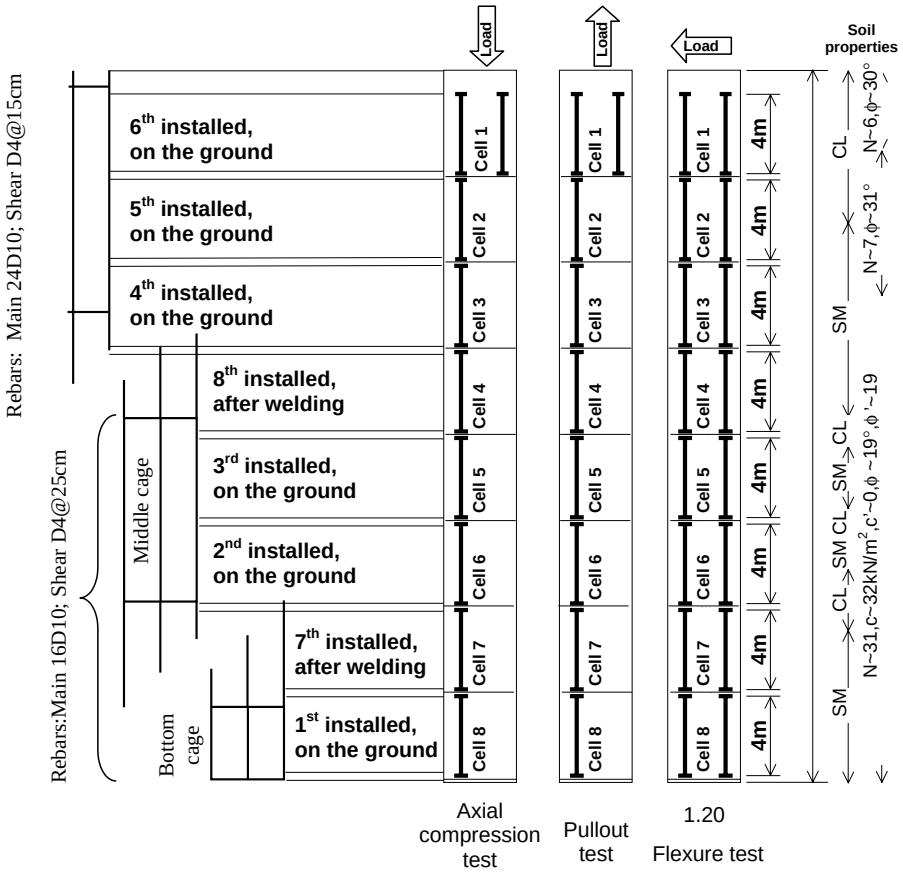

FIGURE 1 Pile dimensions, soil profile, sensor networks, and sequence of installation on the rebar cages.

TABLE 1 Loading and Measurement Schedule

	PULLOUT TEST		AXIAL COMPRESSION TEST		FLEXURE TEST	
Step	Load [t]	Measurement [min.]	Load [t]	Measurement [min.]	Load [t]	Measurement [min.]
0	0.0	0	0	0	0	0
1	28.6	0, 2, 5, 10	60	0, 2, 5, 10	10	0, 3, 6, 10
2	57.1	0, 2, 5, 10	120	0, 2, 5, 10	20	0, 3, 6, 10
3	85.7	0, 2, 5, 10	180	0, 2, 5, 10	30	0, 3, 6, 10, 15, 20
4	114.3	0, 2, 5, 10	240	0, 2, 5, 10	40	0, 3, 6, 10, 15, 20
5	142.9	0, 2, 5, 10	300	0, 2, 5, 10	50	0, 3, 6, 10, 15, 20
6	171.4	0, 2, 5, 10	360	0, 2, 5, 10	60	0, 3, 6, 10, 15, 20
7	200.0	0, 2, 5, 10	420	0, 2, 5, 10	70	0, 3, 6, 10, 15, 20
8	228.6	0, 2, 5, 10	480	0, 2, 5, 10	80	0, 3, 6, 10, 15, 20
9	257.1	0, 2, 5, 10	540	0, 2, 5, 10	90	0, 3, 6, 10, 15, 20
10	285.7	0, 2, 5, 10	600	0, 2, 5, 10	100	0, 3, 6, 10, 15, 20, 40, 60
11	314.3	0, 2, 5, 10	660	0, 2, 5, 10	75	0, 3, 6, 10
12	342.9	0, 2, 5, 10	720	0, 2, 5, 10	50	0, 3, 6, 10
13	371.4	0, 2, 5, 10	780	0, 2, 5, 10	25	0, 3, 6, 10
14	400.0	0, 2, 5,10, 20, 30, 40, 60	840	0, 2, 5, 10, 20, 30, 40, 60	0	0, 3, 6, 10, 15, 20
15	300.0	0, 2, 5, 10	630	0, 2, 5, 10		
16	200.0	0, 2, 5, 10	420	0, 2, 5, 10		
17	100.0	0, 2, 5, 10	210	0, 2, 5, 10		
18	0.0	0, 2, 5, 10, 20, 30, 40, 60	0	0, 2, 5, 10, 20, 30, 40, 60		

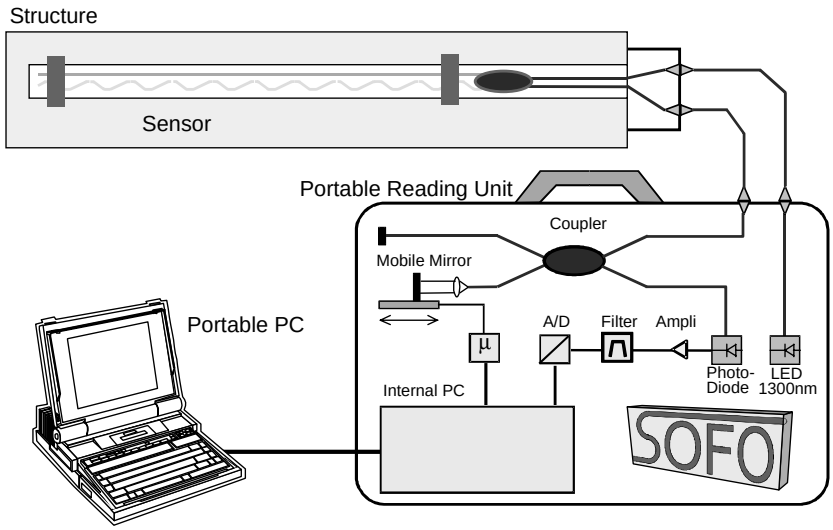

FIGURE 2 Components and functional principle of the SOFO system.

principle of the SOFO system is presented in Figure 2 and pictures of components can be found in Figure 3. The SOFO system consists of sensors, a reading unit, and data acquisition and analysis software. The sensor consists of two optical fibers, the measurement fiber and the reference fiber, contained in the same protection tube. The measurement fiber is coupled with the host structure and follows the deformations of the structure. In order to measure shortening as well as elongation, the measurement fiber is prestressed to 0.5%. The reference fiber is loose and therefore independent from the structure's deformations; its purpose is to compensate thermal influences to the sensor. The optical signal (light) is sent from the reading unit through a coupler to the sensor, where it reflects off mirrors placed at the end of each fiber and returns back to the reading unit where it is demodulated by a matching pair of fibers. The returned light contains information concerning the deformations of the structure, which is decoded in the reading unit and visualized using a portable PC. Typical sensor length (gauge length) ranges from 200 mm to 10 m, while the resolution reaches 2 μm independently from the gauge length and with an accuracy of 0.2%. The dynamic range of the sensors is 0.5% in compression and +1.0% in elongation.

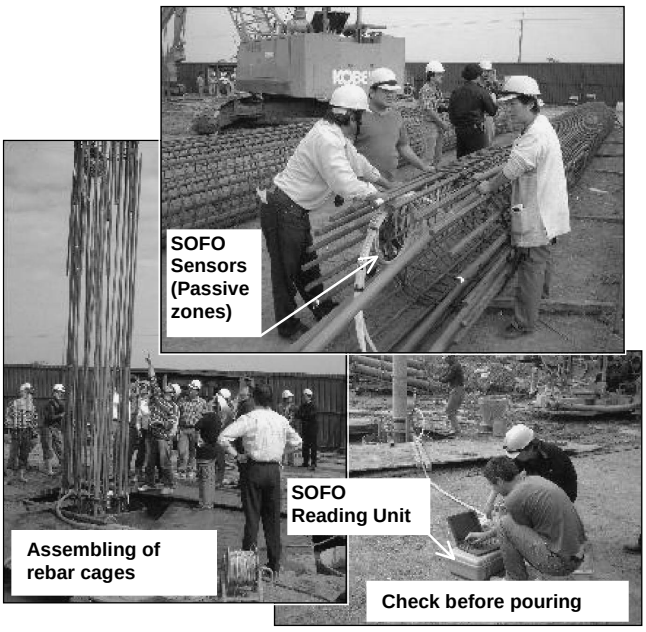

FIGURE 3 Installation of sensors on the rebar cages.

The SOFO system was developed in early 1990s and since 1995 it was commercialized and applied to the monitoring of a wide range of civil structures, such as geotechnical structures, bridges, dams, and residential and industrial buildings, just to name a few (*3*–*6*). The system is insensitive to temperature changes, electromagnetic fields, humidity, and corrosion, and immune from drift for at least 5 years, making it ideal for both short- and long-term monitoring. Being designed for direct embedding in concrete, the sensors allow easy installation, require no calibration, and feature high survival rate (better than 95% for concrete embedding). The long gauge length makes them more reliable and accurate than traditional strain sensors, averaging the strain over long bases and not being influenced by local defects in material (e.g., cracks and air pockets). More information on the SOFO system and its applications can be found in the references (*6*).

For the presented application, 4-m-long sensors were selected. The pile was divided into eight zones (called cells). In the axial compression and pullout tests, a simple topology was used: the eight sensors were installed in a single chain, placed along the main rebar, one sensor in each cell, as shown in Figure 1. To detect and compensate for a possible load eccentricity, the top cell was equipped with one more sensor installed on the opposite rebar with respect to the pile axis (see Figure 1).

In the flexure test, a parallel topology was used: each cell contained two parallel sensors installed on two opposite main rebars, constituting two chains of sensors, as shown in Figure 1. The position of the sensors in the pile's cross section is selected in such a way that the load direction and the sensors are aligned (see Figure 1). From the deformations measured by the sensors, it was possible to calculate the average curvature of each cell, and to retrieve the horizontal displacement at each depth of the pile by double integration of measured curvatures (*7*).

The rebar cage of these piles was too long to be put into the borehole at once. It was therefore split into three sections, which were lowered sequentially and assembled by welding. The sensors were first installed on each section and the sensors whose position corresponded to a welded region were installed after welding, while lowering the cage. The sequence of sensor installation is schematically presented in Figure 1 and pictures taken during installation are shown in Figure 3.

AXIAL COMPRESSION AND PULLOUT TESTS: RESULTS AND ANALYSIS

The full presentation and discussion of each measured parameter largely exceed the scope of this article; therefore, only the most significant results for each particular test are presented. The analyses and the results, which are not similar for the different tests, are mentioned but not detailed.

Average Strain Distribution

The average strain in each cell of a pile was determined as the ratio between the measured deformation (elongation or shortening) and the length of the sensor. This parameter served as a basis to calculate all other parameters. The distribution of the average strain over the length of the pile, in the axial compression test, on the east-side pile for increasing loads is presented in Figure 4 and for decreasing loads in Figure 5. The same diagrams obtained in the case of the pullout test are presented in Figures 6 and 7, respectively.

In Figure 4, a soil layer with poor mechanical properties was identified (encircled area). In this layer the average strain in pile is constant, indicating that either the friction between the pile and the soil is low, or the stiffness/strength of the soil is low, or the cross section of the pile is restricted. Ultrasonic tests confirmed that the cross section of the pile did not change, and therefore this anomaly is most probably the result of the poor mechanical properties of soil at that particular depth.

In Figure 6, a sudden increase in the strain magnitude was noticed. It was the consequence of crack formation and allowed the detection of damage (cracking) and its propagation along the pile, as a function of the load magnitude. When the maximal load was applied, cracks appeared in the first three cells.

Determination of Compressive and Tensional Young Modulus

The Young modulus of the pile is determined during the axial compression and pullout tests. During both tests, the average strains in the first and the second cells were approximately identical for lower loads, which indicated that the soil friction in the first cell could be neglected. Hence the Young modulus for each pile was calculated as a ratio between applied stress and average strain in the first cell. The behavior of piles under the axial compression test was linear, and the value of the Young modulus ranged from 30 to 50 GPa. The piles subjected to traction had approximately bilinear or trilinear behavior during loading and nonlinear behavior during unloading. The stress-strain diagram obtained from measurements on the east-side pile during the pullout test is presented in Figure 8. A sudden decrease in Young modulus was clearly observed after concrete cracking (compare with Figure 6).

Distribution of Average Normal Forces

The average normal (compressive or tensile) force in the pile is determined as the product of the average strain, cross-section area, and calculated Young modulus. In the axial compression tests, being the Young modulus constant, the compressive force distribution diagram is proportional to the one presenting the strain distribution (see Figures 4 and 5).

The tensile force distribution diagram for the pullout test is presented in Figure 9. It has been determined by taking into account the stress–strain dependence presented in Figure 8. The soil layer with poor mechanical properties was once again detected. Since its position is slightly different from that determined by the axial

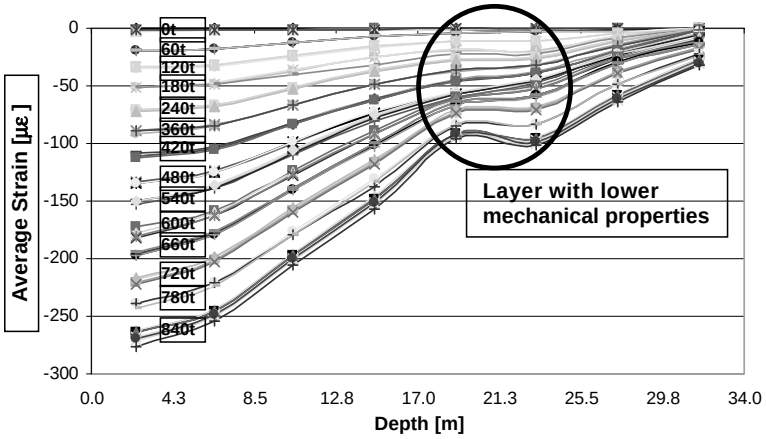

FIGURE 4 Average strain distribution, for increasing loads, axial compression test, east-side pile.

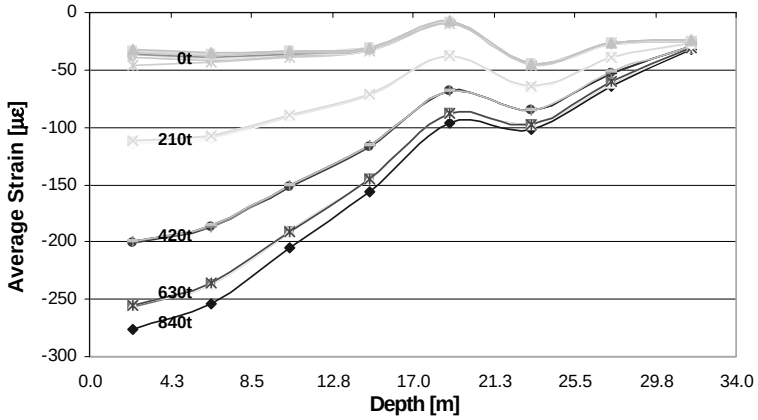

FIGURE 5 Average strain distribution, for decreasing loads, axial compression test, east-side pile.

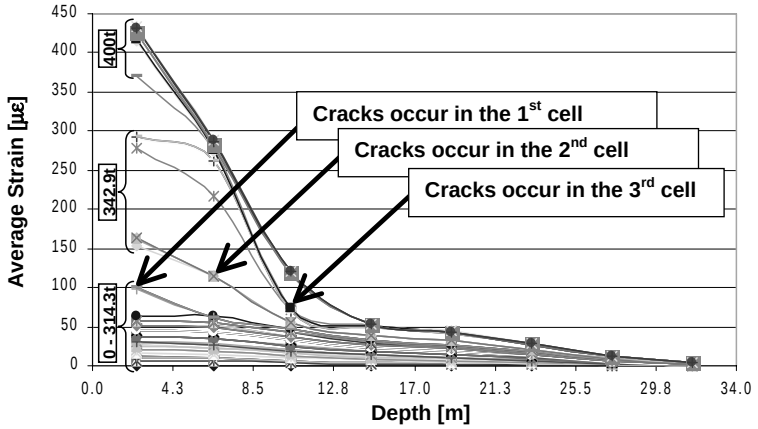

FIGURE 6 Average strain distribution, for increasing loads, pullout test, east-side pile.

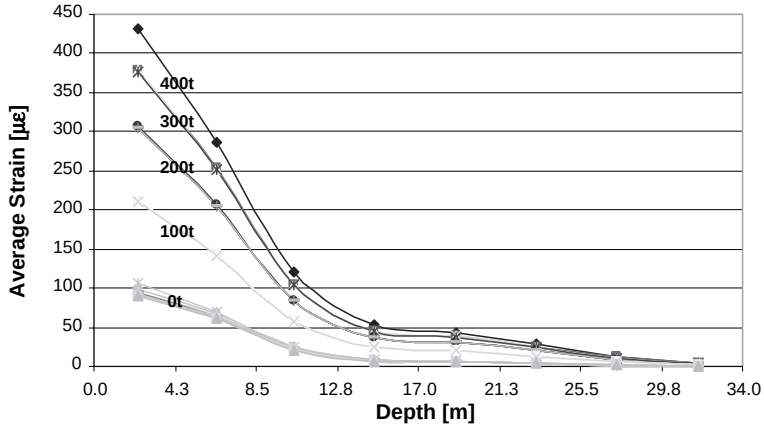

FIGURE 7 Average strain distribution, for decreasing loads, pullout test, east-side pile.

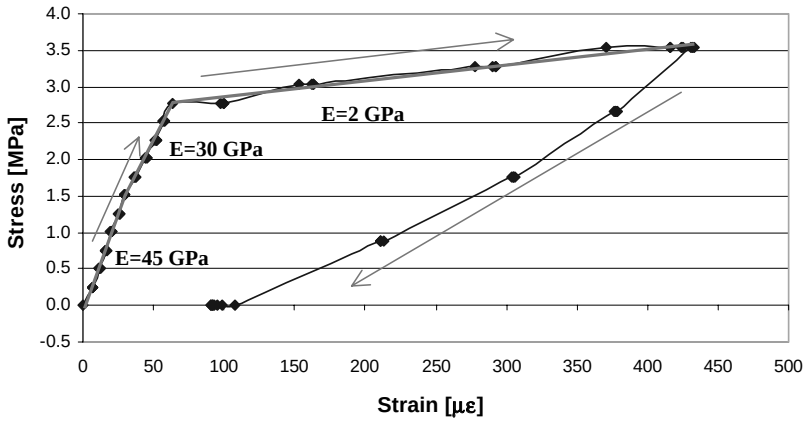

FIGURE 8 Stress–strain diagram for the east-side pile under pullout test.

compression test (see Figure 4), the authors presume that this layer is situated in the lower part of the fourth and upper part of the fifth cell. This statement also explains the nonconstant value of the force in the pile surrounded by soil with poor mechanical properties.

Determination of Ultimate Load Capacity and Tip Displacement

The ultimate load capacity of the pile subjected to compression has been determined as the minimal load causing failure of the lateral friction. It was determined as the load that significantly increases the slope on the tip force versus load diagram. When this slope significantly increases, the pile starts to slip and the tip force is activated. The slippage of the pile was also confirmed by the pile-head displacement measured by LVDT. The determination of the ultimate load capacity as well as the bottom force versus load diagram is presented in Figure 10. The bottom force was assumed to be approximately equal to the compressive force in the bottom cell.

When the pile is exposed to traction, the ultimate uplift capacity is determined as the minimal load that damages the pile. It is clearly observed in Figure 6. This load significantly increases the slope on the pile-head vertical displacement versus load diagram, since the cracks open and the Young modulus decreases. The pile-head displacement was measured using the LVDT, but was also calculated from deformations measured by fiber optic sensors. To simplify the calculation, it was assumed that the pile tip did not move. The pile-head displacement, as well as the determination of the ultimate uplift capacity, is presented in Figure 11. In this diagram the difference between LVDT and SOFO measurements represents the slippage of the pile.

Comparisons between calculated (predicted) bearing capacities and ultimate capacities of piles obtained from tests showed that the short-term safety factors were not satisfactory (1.32 instead of 2.00 for compression and 1.56 instead of 3.00 for uplift) and therefore the pile design must be changed. Both the pile-soil friction surface and the total pile traction strength must be increased.

Distribution of Pile–Soil Friction

To simplify determination of the pile–soil lateral friction, the following assumptions were adopted:

- Normal stress and strain are constant in the pile cross section.
- Friction is constant between the centers of neighboring cells.

Consequently the normal force change is linear as well as the normal stress and strain.

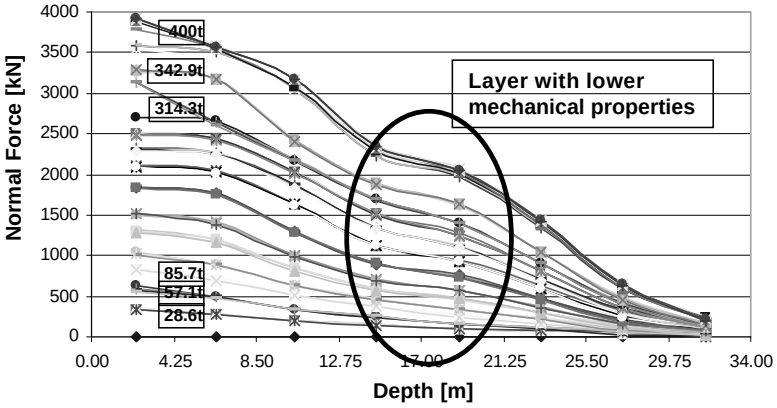

FIGURE 9 Tensile force distribution for east-side pile under pullout test, for increasing loads.

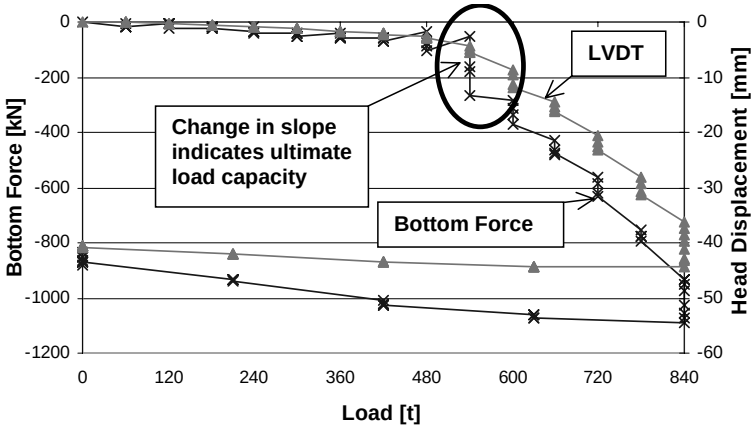

FIGURE 10 Tip force versus load diagram and determination of ultimate load capacity of the east-side pile, under axial compression test.

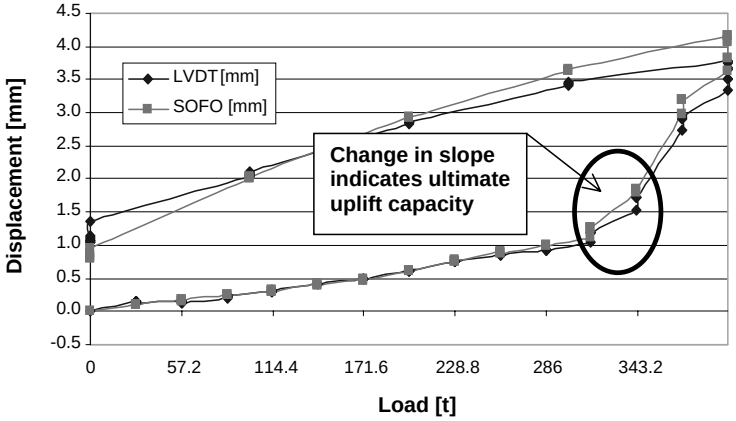

FIGURE 11 Head displacement versus load diagram and determination of the ultimate uplift capacity of the east-side pile, under pullout test.

• Geometrical and mechanical properties of the pile do not change with the length of the pile. This assumption is necessary to simplify the analysis even if it is not entirely correct. On one hand, the diameter certainly varies slightly due to the construction method, and on the other hand, the density of rebars is not constant over the length of the pile.

The first two assumptions are schematically represented in Figure 12.

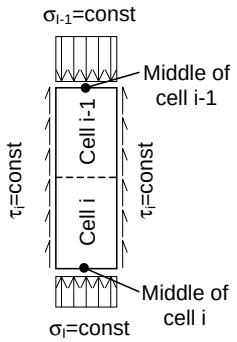

FIGURE 12 Assumed stress and friction distribution in one section of the pile embedded in soil layer *i*.

The calculated distribution of pile–soil friction for axial compression at the ultimate load capacity (480 tons) and at the maximal applied load (840 tons) is presented test in Figure 13. Three zones of soil with different mechanical properties are identified and highlighted in this figure. While the first and the third zone have good mechanical properties, the mechanical properties of the second zone are significantly lower.

FLEXURE TEST: RESULTS AND ANALYSIS

Average Strain in Piles

During the flexure test, the order of magnitude of the average strain varied between 0 με in Cell 8 and 1,000 με in Cell 2. The average strain with respect to load is presented in Figure 14. For practical reasons, the average strain distribution is presented with respect to the load, and not with respect to the depth of the sensor as in the case of axial compression and pullout test.

A high difference in the strain magnitude for the different cells can be observed in Figure 14. Cell 2 was the most deformed, followed by Cells 1 and 3, whereas Cells 4 to 8 were practically

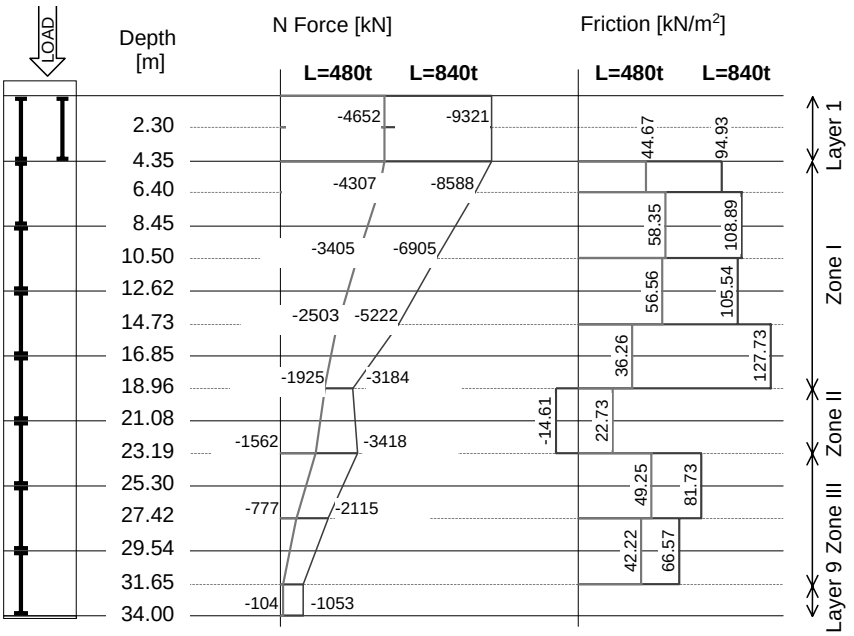

FIGURE 13 Distributions of the normal force in the pile, friction stress, and different layers of soil (L = load).

unaffected, even for the maximal applied load. For loads below 50 tons, parallel sensors installed in each cell measured approximately the same absolute value of deformation. This means that for those loads the pile was not cracked. For higher levels of load, an asymmetry is observed due to cracking and the consequent displacement of the neutral axis.

Average Curvature and Displacement

The average curvature in each pile cell was calculated from the average strain assuming that the Bernoulli hypothesis is satisfied (plane cross sections of the pile remain plane under loading) (*7*). The average curvature with respect to the load for the first four cells is presented in Figure 15. The curvature of the fourth cell an practically be neglected. The same is true for Cells 5 to 8, and that is why the average curvature for these cells is not presented in Figure 15.

The deformed shape (horizontal displacement) of pile was calculated using a double integration of the curvature function (*7*), and is presented in Figure 16. Again, the maximal displacement is observed in the first three cells of the pile. The point with maximal curvature in the Figure 16 corresponds to the failure point of the pile (plastic hinge).

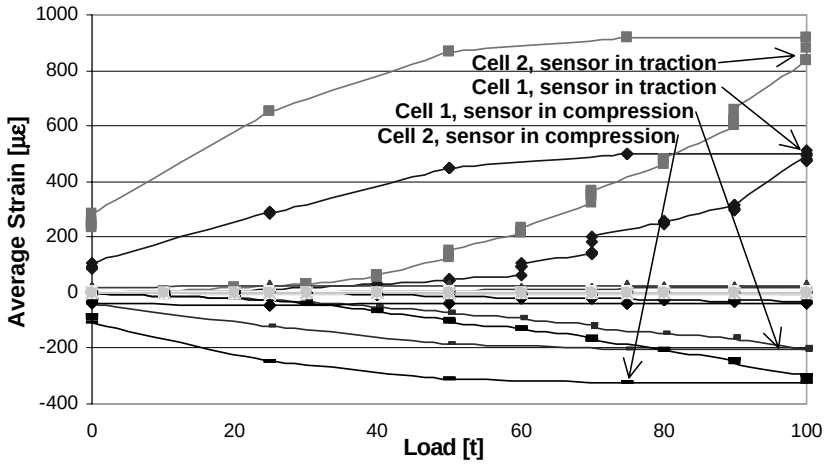

FIGURE 14 Average strain with respect to load, flexure test, in west-side pile.

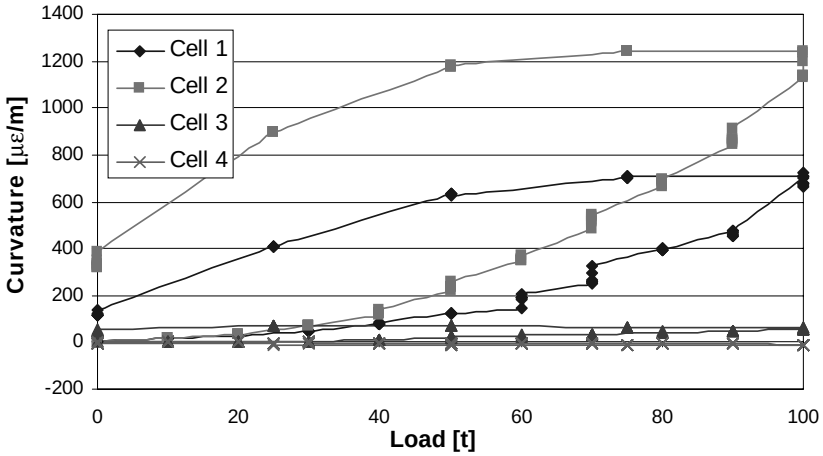

FIGURE 15 Average curvature with respect to load, flexure test, in west-side pile.

Ultimate Lateral Load Capacity and Failure Localization

The ultimate lateral load capacity of the pile was identified as the minimal load that generates cracking in the pile. According to Figures 14 to 16, this load is situated between 40 and 50 tons. The pile failed at the depth of approximately 10 m, according to Figure 16.

CONCLUSIONS

The foundation performances determined using the long-gauge fiber optic sensors are presented in Table 2. The Young modulus ranged between 45 and 50 GPa, with the exception of the east-side pile tested on compression, where the Young modulus was lower (30 GPa). The maximal traction strain of concrete determined during pullout and flexure tests is approximately equal for all piles and corresponds to 60 με. The traction strength of the concrete is therefore estimated to be about 2.7 to 3 MPa. Since the mechanical properties were relatively uniform among all piles, it can be concluded that their quality was identical.

The tests helped to understand the real foundation behavior and to evaluate its performance, to determine failure mode, and to localize cracking zones and failure points. In addition, mechanical properties of soil were determined and globally three layers with different properties were distinguished at both the east and the west sites. The ultimate load capacity for all tests was approximately equal to half of the maximal applied load, which is in agreement with the design values.

In future applications of the presented technique and in order to determine the Young modulus and the tip force more accurately, the authors recommend the use of shorter sensors (1 to 2 m) in the first and last cell.

ACKNOWLEDGMENTS

The authors would like to thank Fu Tsu Construction Co., the contractor, as well as Bovis Lend Lease Microelectronics, the general consultant, for their professional collaboration and kind courtesies.

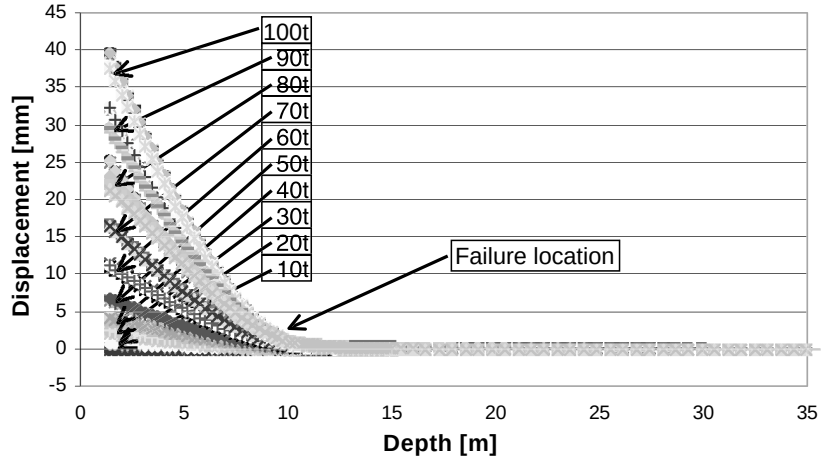

FIGURE 16 Deformed shapes of the pile, flexure test, in west-side pile.

TABLE 2 Foundation Performances Determined Using Long-Gauge Fiber Optic Sensors

	PULLOUT TEST	AXIAL COMPRESSION TEST	FLEXURE TEST
Young modulus of pile	E=45-50 GPa	E=30-50 GPa	Not calculated
Deformation of pile	Average longitudinal strain distribution Distribution of vertical displacement	Average longitudinal strain distribution Distribution of vertical displacement	Average longitudinal strain distribution Distribution of curvature Distribution of horizontal displacement (deformed shape)
Forces in pile	Distribution of tensile force Bottom force	Distribution of compressive force Bottom force	Qualitative distribution of bending moments
Strain when cracks occur	ε=60με	No crack detected	ε=60με
Damaging of pile	Detection of crack occurring Localization of zone affected by cracking	No damaging detected	Detection of crack occurring Localization of zone affected by cracking
Properties of soil	Qualitative determination of soil strength Identification of zones with different mechanical properties	Qualitative determination of soil strength Identification of zones with different mechanical properties	Qualitative determination of soil strength
Forces in soil	Distribution of pile-soil friction	Distribution of pile-soil friction	Distribution of horizontal reactions of soil
Failure mode	On pile (cracking)	On soil (slip)	On soil (first) and pile (afterwards)
Ultimate load capacity	314.3t to 343.2t	480t to 540t	50t

REFERENCES

1. Inaudi, D., N. Casanova, S. Vurpillot, B. Glisic, P. Kronenberg, and S. LLoret. Lessons Learned in the Use of Fiber Optic Sensor for Civil Structural Monitoring. *Proc., 6th International Workshop on Material Properties and Design*, Bauhaus University Weimar, Weimar, Germany, Sept. 2000, pp. 79–92.
2. Inaudi, D. *Fiber Optic Sensor Network for the Monitoring of Civil Structures*. Ph.D. thesis. EPFL, Lausanne, Switzerland, 1997.
3. Inaudi, D., and N. Casanova. Geo-structural Monitoring with Long-Gauge Interferometric Sensors. *Proc., SPIE, 7th International Symposium on Smart Structures and Materials*, Newport Beach, Vol. 3995, March 2000, pp. 164–174.
4. Glisic, B., M. Badoux, J.-P. Jaccoud, and D. Inaudi. Monitoring a Subterranean Structure with the SOFO System. *Tunnel Management International*, Vol. 2, No. 8, 2000, pp. 22–27.
5. Glisic, B., D. Inaudi, P. Kronenberg, and S. Vurpillot. Dam Monitoring Using Long SOFO Sensor. In *Hydropower into the Next Century*. Gmunden, Austria, Oct. 18–20, 1999, pp. 709–717.
6. SMARTEC SA. Bibliography. smartec.ch/home.htmsmartec.ch.
7. Vurpillot, S. *Analyse Automatisée des Systèmes de Mesure de Déformation pour L'auscultation des Structures*. Ph.D. thesis. EPFL, Lausanne, Switzerland, 1999.

Publication of this paper sponsored by Committee on Soils and Rock Instrumentation.